AUTONOMOUS VEHICLES

A hybrid underwater robot for multidisciplinary investigation of the ocean twilight zone

Dana R. Yoerger[1]*, Annette F. Govindarajan[1], Jonathan C. Howland[1], Joel K. Llopiz[1], Peter H. Wiebe[1], Molly Curran[1], Justin Fujii[1], Daniel Gomez-Ibanez[1], Kakani Katija[2], Bruce H. Robison[2], Brett W. Hobson[2], Michael Risi[2], Stephen M. Rock[3]

***Mesobot*, an autonomous underwater vehicle, addresses specific unmet needs for observing and sampling a variety of phenomena in the ocean's midwaters. The midwater hosts a vast biomass, has a role in regulating climate, and may soon be exploited commercially, yet our scientific understanding of it is incomplete. *Mesobot* has the ability to survey and track slow-moving animals and to correlate the animals' movements with critical environmental measurements. *Mesobot* will complement existing oceanographic assets such as towed, remotely operated, and autonomous vehicles; shipboard acoustic sensors; and net tows. Its potential to perform behavioral studies unobtrusively over long periods with substantial autonomy provides a capability that is not presently available to midwater researchers. The 250-kilogram marine robot can be teleoperated through a lightweight fiber optic tether and can also operate untethered with full autonomy while minimizing environmental disturbance. We present recent results illustrating the vehicle's ability to automatically track free-swimming hydromedusae (*Solmissus* sp.) and larvaceans (*Bathochordaeus stygius*) at depths of 200 meters in Monterey Bay, USA. In addition to these tracking missions, the vehicle can execute preprogrammed missions collecting image and sensor data while also carrying substantial auxiliary payloads such as cameras, sonars, and samplers.**

INTRODUCTION

Scientific exploration of the ocean's twilight zone

The ocean's midwater realm represents a challenging frontier for underwater robots. The ocean's midwater or "twilight zone" teems with life and extends from about 200 to about 1000 m in depth. At depths below the upper bound, light levels are insufficient to support photosynthetic primary productivity, whereas at the lower bound, conditions are effectively aphotic (*1*). This vast region hosts abundant life and plays a key role in the global carbon cycle, thereby regulating Earth's climate and the biogeochemistry of its oceans. Technological limitations currently constrain our ability to study patterns and processes in this region. Existing marine robots excel at tasks such as efficient seafloor and water column survey and can conduct such surveys to the oceans' greatest depths. However, the midwater presents different opportunities and challenges, such as making long-duration observations of sensitive animals without disturbing them. Long-term observation (on the order of a day) will favor an approach that minimizes the role of the surface vessel; in contrast, our best present-day midwater observation assets (remotely operated and human-occupied vehicles) must be tended continuously by the surface vessel.

Interest in the twilight zone is growing as the vastness of its biomass and biodiversity become more apparent. Certainly, exploration of one of Earth's largest, least understood, and most diverse ecosystems can be motivated by basic scientific interests alone, but other more specific considerations are also emerging. Recent estimates suggest that midwater fish biomass may be 100 times larger than the total fish biomass harvested globally every year (*2*), and exploratory mesopelagic fisheries have recently been undertaken in many locations (*3*). Although midwater fish species differ markedly from the pelagic fish traditionally exploited for human consumption, midwater animals could find commercial markets in products like fish meal for agriculture and aquaculture, as well as other products like "nutraceuticals" such as fish and krill oil (*4*). Interest in the midwater ocean is also motivated by understanding how it supports species living in near-surface waters and its role in regulating Earth's climate. Recent observations obtained using tags confirm that many charismatic epipelagic species—such as whales, sharks, swordfish, and tuna—dive regularly into the twilight zone to feed on abundant populations of animals such as squid (*5*–*7*). Likewise, midwater animals likely play a major role in transferring carbon from near-surface waters to the deep ocean, as part of the "biological pump" (*8*–*10*). These activities may mitigate the effects of rising atmospheric CO_2, but the precise mechanisms involved and their global importance are not well understood.

Many midwater animals undertake diel (daily) migrations, spending daylight hours at hundreds of meters depth, presumably to avoid predation; rising to near-surface waters at night to feed in the cover of darkness; and then descending to safer, darker waters at daybreak (*11*). Some of these animals can be observed indirectly from vessel-mounted sonars, forming the "deep scattering layer" (*11*). This phenomenon occurs between about 60N and 60S latitude and occurs around the globe each day. This daily movement of animals results in the largest migration on Earth (*12*). When these animals feed near the surface then defecate after they retreat to deeper water, they physically carry organic carbon from shallow to deep water. However, the details of how much carbon is actually sequestered via these biological processes remain uncertain (*12*–*14*).

Guided by present and future community research priorities, we have developed a robot (Movie 1) that enables unique scientific access to midwater environments, complementing other tools currently available. The detailed vehicle attributes were developed within our interdisciplinary group and discussed with a larger midwater research community at several international meetings. Specifically,

[1]Woods Hole Oceanographic Institution, Woods Hole, MA 02543, USA. [2]Monterey Bay Aquarium Research Institute, Moss Landing, CA 95039, USA. [3]Department of Aeronautics and Astronautics, Stanford University, Stanford, CA 94305, USA.
*Corresponding author. Email: dyoerger@whoi.edu

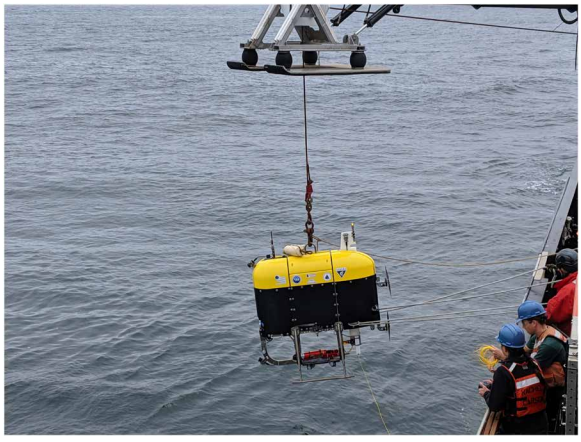

Movie 1. Summary video. Overview of *Mesobot*'s development and at-sea tracking capabilities.

we identified the need for a vehicle that could enable behavioral studies that are difficult with our current assets, with low avoidance/attraction and the ability to operate independently from the support vessel. We report here on the design, construction, and testing of *Mesobot*, which will advance our understanding of the daily lives of midwater animals by observing them over extended periods of time (hours to a day). Although human-occupied and remotely operated vehicles (ROVs) can operate very effectively in midwater (*15*), hybrid (*16*, *17*) or fully autonomous vehicles have distinct advantages especially for long-duration tracking missions while imposing lower demands on the support vessel. In addition to automatically tracking animals with minimal disruption, *Mesobot* can perform a variety of midwater surveys, such as video transects. The vehicle carries a full suite of oceanographic sensors and can perform preprogrammed, targeted, or adaptive surveys (*18*). The vehicle also has substantial capacity (~20 kg of in-water weight, ~0.1 m^3) for auxiliary specialized payloads, such as plankton imaging systems, sonars, and samplers. Such observations from a hybrid vehicle will enable studies of behavior that until now were difficult to achieve.

Midwater exploration technology and the role of *Mesobot*

A variety of technologies have been used for midwater studies. These include in situ sensors, nets, acoustic echo sounders, water samplers, and a wide variety of specialized camera systems (*9*, *15*, *19*). Such devices are typically lowered on a cable or towed behind a vessel although, in recent years, they have been deployed on human-occupied, remotely operated, and autonomous vehicles. *Mesobot* was conceived to complement and fill important gaps not served by these existing technologies and platforms.

Much of what we know about midwater biota has been learned by towing or lowering nets. A wide variety of nets have been devised, each with specific capabilities (*19*). Although essential for midwater studies, nets have many limitations. Many animals actively avoid capture, so any particular net tow may not provide an accurate representation of the diversity or abundance over the volume sampled (*20*). Likewise, nets may destroy many species of gelatinous zooplankton. Operations with nets fully occupy the research vessel while deployed, and processing of samples is labor intensive. However, obtaining specimens will be necessary for the foreseeable future to enable taxonomic studies, to develop detailed studies of food webs and life histories, and to build genetic barcode libraries that will in turn enable the presence and perhaps abundance of particular organisms to be determined from environmental DNA (*21*).

In recent years, nets have been supplemented with specialized camera systems to observe midwater biota such as zooplankton (*22*–*25*). Such cameras have been used on towed platforms, powered autonomous underwater vehicles (AUVs), and profiling moorings. Several different optical designs have emerged, each making different tradeoffs between image quality, volume, and depth of field. Image quality for these systems can be very high, and combined with automated image processing, they can survey substantial volumes effectively. These imaging systems generally provide snapshots of the targets and are rarely operated in such a way that they can observe individual animals for extended periods of time as required for behavioral studies.

Echo sounders—either vessel mounted, towed, lowered, or moored—also provide valuable data on midwater species. Vessel-mounted echo sounders are the dominant remote-sensing methodology for midwater studies, allowing large volumes to be scanned efficiently. Many efforts are underway to make these acoustic systems better able to identify species and obtain accurate estimates of biomass and biodiversity (*26*–*28*).

The oceanographic community uses many vessel-deployed and fully autonomous instruments and platforms to survey the midwater ocean. Conductivity, temperature, and depth profilers (CTDs) are lowered from research vessels on a cable. Modern CTDs now include a wide variety of other instruments and water sampling. Since 2000, thousands of fully autonomous profiling Argo floats, actuated by buoyancy engines, have been deployed worldwide. They have provided unprecedented data on a range of topics including ocean circulation, air-sea interaction, and climate change (*29*). Gliders carry similar instruments and are actively mobile; they profile and move laterally using a combination of a buoyancy engine, wings that supply lift, and control of their attitude by shifting their center of gravity (*30*). Long-range AUVs (*31*, *32*) combine attributes of powered AUVs and gliders to perform surveys over thousands of kilometers with many weeks of endurance. Swarming underwater drifters (M-AUEs, mini-autonomous underwater explorers) are also emerging to survey the midwater ocean (*33*). ROVs are routinely used to observe and sample midwater animals, conduct manipulative experimental work, perform acoustic and visual surveys, and enable behavioral studies while attended by a surface vessel (*15*). The sensor payloads carried by remotely operated and autonomous vehicles have expanded in recent years and now include fluorometers, echosounders for bioacoustics, and even mass spectrometers.

Any marine robotic platform will disrupt the environment to some extent, causing some animals to flee while attracting others. Although skillful operation of human-occupied vehicles or ROVs can result in close-up observations of even very sensitive animals (*9*, *15*, *34*), platforms that can more robustly observe animals while minimizing animal disturbance are still needed. Animal behavioral responses can be evoked because of many factors, including lighting, hydrodynamic disturbances, acoustics, electromagnetic fields, or a vehicle's chemical signature. Although all relevant factors cannot be eliminated, they can be greatly reduced. Ambient light levels and spectral characteristics must be considered when trying to observe biology in the mesopelagic, where animal activity is strongly driven by light of varying sources (*35*). Even in the greater depths of the mesopelagic where light levels are extremely low (9 to 10 orders

of magnitude lower than on the surface), light appears to strongly drive animal behavior (*36*–*38*). Although artificial illumination for imaging can be disruptive, these deleterious effects can be reduced (*39*) using lights with longer wavelengths (e.g., red, near infrared) to which many deep sea animal visual systems have minimal sensitivity (*40*–*42*). Many marine animals, including fish and invertebrates, are highly sensitive to hydrodynamic disturbances. As is the case with an underwater vehicle, an approaching predator generates a bow wave that can elicit escape responses in fish even in the dark (*43*). Likewise, invertebrates respond to hydrodynamic disturbances to maintain aggregations (*44*) and to avoid predation (*45*), and delicate gelatinous zooplankton can be damaged by the bow wave or thruster activity of an approaching vehicle (*15*). Technical solutions to minimize these effects include providing the vehicle with a hydrodynamic shape, equipping the vehicle with low-powered thrusters that turn large, slow-moving propellers that do not direct flow into the imaging volume, minimizing and carefully controlling vehicle thrust, and making the vehicle near-neutrally buoyant and uncoupled from surface vessel motions (*46*).

The extent to which a marine robot should resemble typical animals is a topic of debate. Investigators have built marine robots that resemble fish in appearance either to minimize avoidance (*47*) or conversely to resemble predators to actively repel invasive species (*48*). These efforts focus on the robot's appearance in sunlit waters but neglect many of the other mechanisms for avoidance and attraction that have been well documented for mesopelagic animals (*34*). Investigators have also documented how conventional survey AUVs can attract fish, which may follow such a vehicle in large schools (*49*) or even attack the vehicle violently (*50*, *51*). *Mesobot* does not physically resemble any marine organism; rather, its design seeks to minimize all the other known mechanisms that might elicit avoidance or attraction.

Although existing midwater platforms are highly effective for their intended purposes, advances in autonomous vehicle technology hold much promise for enabling longer-duration observations that are conducted less obtrusively, at lower cost, and while operating more independently from surface vessels (*52*). Our goals are to supplement or complement rather than replace the capabilities described earlier. Accordingly, we conceived *Mesobot* (Fig. 1), which has the following attributes:

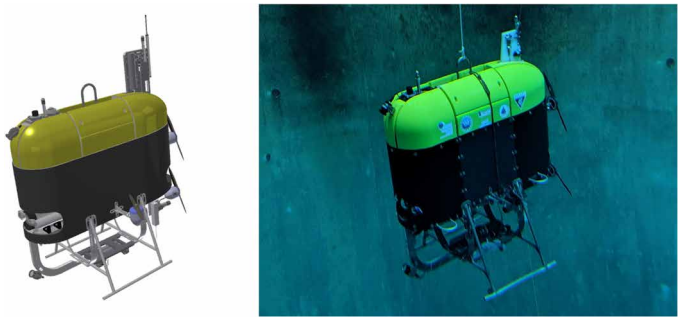

Fig. 1. *Mesobot* rendering and photo. *Mesobot* is a hybrid underwater vehicle designed to follow slow-moving midwater targets such as zooplankton, fish, and particle aggregates. The vehicle carries stereo cameras for target tracking and a high-quality video/still camera for scientific documentation. *Mesobot* is 1.5 m tall and displaces about 250 kg.

1) The vehicle shall be able to observe and image targets for extended periods, including slow-moving animals, particulates, aggregates, bubbles, and droplets. Our automated tracking efforts were motivated by previously documented successful efforts with the Monterey Bay Aquarium Research Institute's (MBARI) *Ventana* (*53*) and Japan Agency for Marine-Earth Science and Technology (JAMSTEC)'s *PICASSO* (*54*) ROV systems. Compared with *PICASSO*, *Mesobot* has greater endurance and larger payload capacity and is capable of fully autonomous operation.

2) The vehicle design shall minimize disturbance of the imaging volume from a hydrodynamic, acoustic, and optical perspective.

3) Similar to many of its targets, the vehicle shall behave "mostly Lagrangian," hovering efficiently and moving with ambient water masses, and maneuver actively with fine control to follow slow-moving targets.

4) The vehicle should have a mission duration exceeding 24 hours to observe diel migrations, with even longer endurance for less energetic tasks such as following oceanographic features and sampling.

5) The vehicle should work to a depth of 1000 m, enabling the vehicle to track most diel migrators and putting many important mesopelagic scientific problems within its reach.

6) The vehicle should be able to carry auxiliary payloads such as specialized plankton imaging system, sonars, or samplers to carry out a range of midwater survey tasks such as exploratory surveys; providing ground-truth for acoustic surveys; and following features such as isotherms, isopycnals, or neutral surfaces.

Typical *Mesobot* mission

Mesobot is a flexible platform capable of a variety of missions and can operate in a tethered or untethered mode. One important dive profile focuses on a mission to track midwater animals over a full diel cycle, including migrating and nonmigrating targets (Fig. 2). In this scenario, we begin by launching the vehicle with a lightweight (3 mm in diameter) fiber-optic tether that is typically about 50 m in length and is weighted so it assumes a stable configuration and does not tangle with the vehicle or clump. The tether is attached to MBARI's SmartClump, which carries a navigational beacon, a depth sensor, cameras, lights, and thrusters that enable its heading to be controlled and provides situational awareness around *Mesobot*. The tether provides a high-bandwidth network connection, enabling a human pilot on the surface to control the vehicle such as an ROV while viewing images from the stereo and science cameras. After finding a suitable target and initiating tracking, the tether can be released from the vehicle and recovered along with SmartClump, and the vehicle will continue to track the target autonomously. Depending on the species and local conditions, the vehicle may descend as deep as 1000 m while following a specific animal. During the dive, the vehicle can also carry other auxiliary packages such as additional sensors or samplers.

RESULTS

Tracking results in a test tank

We conducted a series of tracking tests in MBARI's seawater test tank facility (10 m in width, 13 m in length, and 10 m in depth). In these tests, we used a simulated target (the Shacklefish; see fig. S1) that could be moved manually throughout the tank. We evaluated *Mesobot*'s ability to intercept and follow a target moving vertically through the imaging volume using the Shacklefish to simulate how

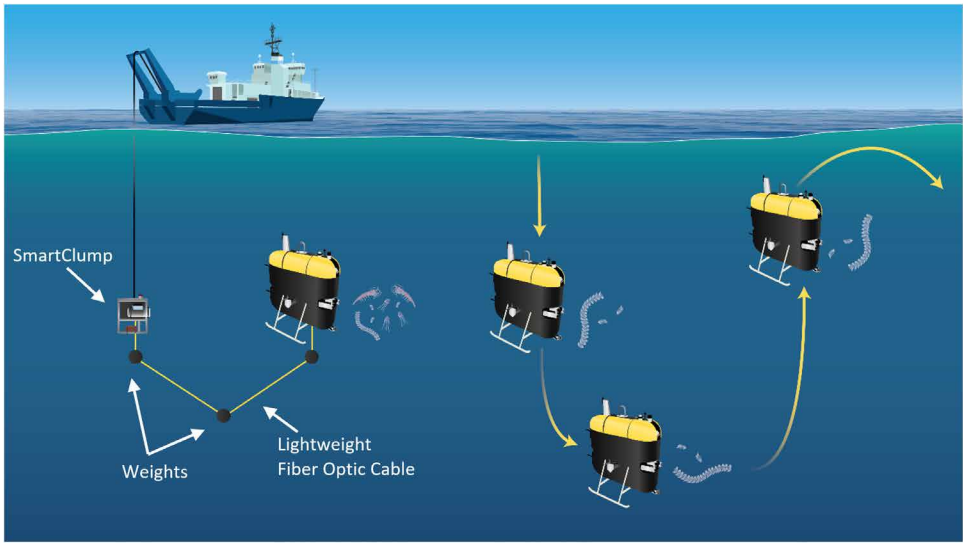

Fig. 2. Typical *Mesobot* tracking mission. Tracking missions will begin with a teleoperated phase, where the vehicle is controlled by a human pilot via a tether and an intermediate vehicle such as MBARI's SmartClump. After locating a suitable target, the tether can be released, and the vehicle will track the target autonomously using its stereo cameras and on-board computers.

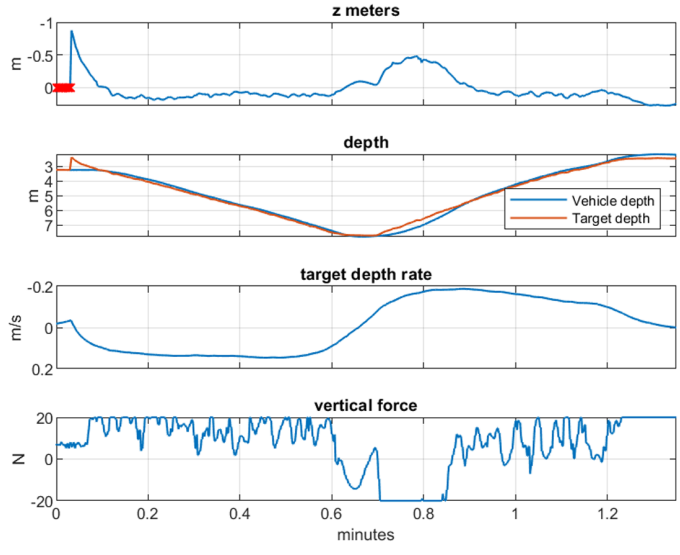

Fig. 3. Tank test performance. These plots summarize tank test performance that illustrate the system's ability to intercept and track a descending target. The top shows the target vertical position in the vehicle frame. At the start, the tracking information is invalid as signified by the red symbols. The tracking information becomes valid when the target enters the top of the field of view. The vertical tracking value immediately converges to a low value as the control system maneuvers the vehicle to bring the target to the center of the visual field. As seen in the second panel, the vehicle begins to descend to track the target, converging to a descent speed of about 15 cm/s. Near the bottom of the tank, the target motion is reversed, and the system tracks the target as it ascends. The vertical force saturates when the target reverses, but the tracking information remains valid, and the target again returns to the center of the visual field.

the vehicle would respond when a migrating animal enters *Mesobot*'s visual field. As shown in Fig. 3, the system performed well in repeated tests with the target either rising or falling at speeds exceeding those of typical migrating zooplankton despite positive vehicle ballasting, which requires more thrust to offset during descent. Running tests at a nominal target speed of about 10 cm/s (360 m/hour), which emulates a high migration speed for typical zooplankton (*55*), we conclude that the vertical response of the control system, including stereo imaging and dynamic control, is sufficient to enable the system to lock onto and follow migrating zooplankton.

Tracking zooplankton in the field

In October 2019, we conducted field trials to test *Mesobot*'s ability to track zooplankton. The tests took place near Moss Landing, CA, USA (36° 45′N and 122° 0.6′W) in water with a bottom depth of ~1000 m. We deployed *Mesobot* from MBARI's research vessel (RV) *Rachel Carson* (*56*) with a 50-m-long and 3-mm-diameter fiber optic tether that was connected to SmartClump (Fig. 2). We deployed *Mesobot* first, drove it away from the vessel on the surface, deployed SmartClump, and then lowered SmartClump while driving the vehicle down. The vessel operators and *Mesobot's* human pilot worked together to ensure that *Mesobot* remained within 50 m of SmartClump to avoid breaking the tether until the tether was released. An ultrashort baseline acoustic tracking system (*57*) and telemetry from both the vehicle and SmartClump enabled the vessel operators and the *Mesobot* pilot to observe their position relative to each other and the vessel (Fig. 2). After reaching an operating depth of 200 m, we began searching for targets, with the human pilot using combinations of auto-heading, auto-depth, and fully manual operation. We encountered and successfully tracked giant larvaceans (*Bathochordaeus stygius*) and "dinner plate" jellyfish (*Solmissus* sp.) (Fig. 4). Both the science camera and the stereo cameras also recorded and demonstrated the capability to track marine snow particles. As we neared the end of the dive, we intentionally released the tether at the vehicle, after which the vehicle continued to track the target autonomously for several minutes as programmed. We recovered SmartClump and *Mesobot* after they returned to the surface autonomously using their thrusters. To avoid any disturbance of the Monterey Bay Marine Sanctuary in which we were operating, we did not release the steel weights as we normally would. Our autonomous emergency responses would have dropped the weights if a major fault occurred or if the battery packs had been depleted.

Solmissus tracking examples

We tracked several *Solmissus* sp., one for nearly 4 min while it descended and another for about 2 min while it moved horizontally. The corresponding tracking and science video are shown in Movie 2. In the descending example, the animal moved actively at an average descent speed of 3.5 cm/s, which is a typical speed for migrating zooplankton (*55*). The video imagery shows the behavior of the animal and allows the animal's body movements to be accurately correlated to its swimming speed. While tracking, the animal exhibited well-known foraging behavior known as "ramming," where the

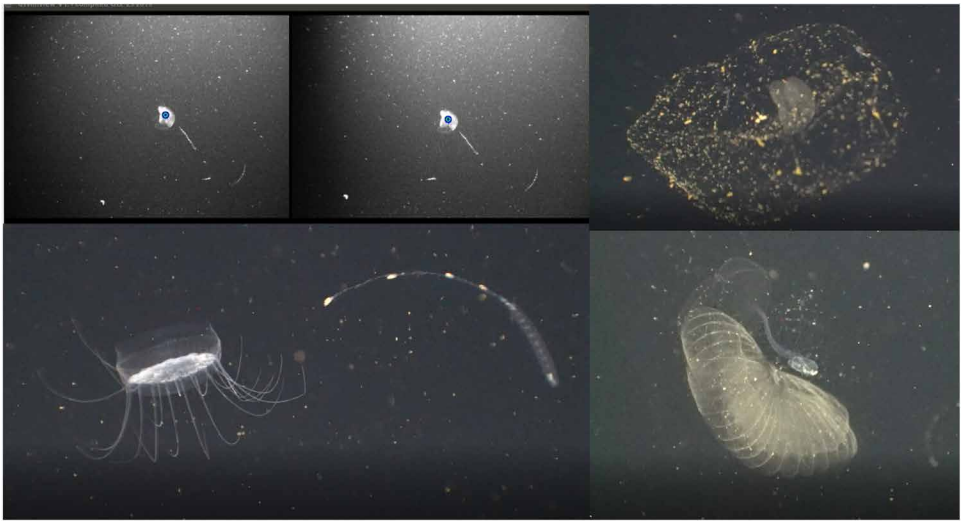

Fig. 4. Typical images from dive Mesobot015. Top left: Real-time tracking display showing left and right camera images while following a *Solmissus* jellyfish; the blue dots indicate the selected left and right targets. Bottom left: A video still from the science camera showing the *Solmissus* while *Mesobot* was tracking automatically, along with a siphonophore and marine snow. Top right: A giant larvacean inside its "outer house." Bottom right: A giant larvacean (which resembles a tadpole) and its "inner house." Larvaceans drive water through their inner house to enable filter feeding. *Mesobot* tracked this target for more than 30 min without disturbing it. Movie 2 is the corresponding *Solmissus* tracking video.

Movie 2. *Solmissus* sp. tracking example. *Mesobot* actively tracking a *Solmissus* jellyfish as it descends at a speed of about 3.5 cm/s. The animal exhibits a feeding behavior known as ramming (*58*) when the animal swims with its venomous tentacles forward to disable and capture prey. In this clip, the *Solmissus* "rams" a siphonophore, but the siphonophore escapes. The tracking algorithm maintained tracking during the ramming incident and while the siphonophore swam away.

animal moves with its venomous tentacles directed forward to capture prey (*58*). At one point in the video, the *Solmissus*' tentacles contact a siphonophore (*Nanomia bijuga*), known prey for *Solmissus* (*58*). In this case, the siphonophore escapes, and the active tracking of *Solmissus* continued.

While tracking the descending animal, the tracking algorithm converged quickly and without overshoot as it did in the examples from the test tank (Fig. 5). The vertical motion was smooth, and the thruster activity was low and exhibited only a very small limit cycle (a few percent of the maximum thrust value of 60 N). Tracking was lost at the end of the run when a large, bright, fast-moving animal (siphonophore) interrupted the tracking. Tracking that is robust to interfering organisms remains a priority for future efforts.

Giant larvacean *Bathochordaeus* tracking example

On the same dive (Mesobot015), we also tracked a giant larvacean, *B. stygius* (*59*), for more than 40 min, including a 30-min continuous segment. Larvaceans are pelagic tunicates that spend much of their lives passively drifting rather than actively swimming. They build mucous structures, commonly referred to as "houses," through which they pump water to enable filter feeding (*60*). These animals play an important role transferring carbon from near-surface waters to the deep ocean (*9*, *10*). The outer house, which often reaches 1 m in size, acts as a prefilter to exclude large particles from clogging the inner house. The outer house is extremely fragile, whereas the sturdier inner house is typically ~20 cm across.

After encountering the larvacean, we approached it carefully and engaged automatic tracking for a few minutes before the extremely fragile outer house began breaking down. While the outer house deteriorated, the vehicle could not maintain tracking due to the complexity of the scene. However, once the outer house was gone, the system achieved very stable tracking on the inner house and the actual animal, as shown in Movie 3 and the still images in Fig. 6. The vehicle tracked the animal for more than 30 min with no signs that the inner house or the animal had been disturbed, as shown in Fig. 6 and Movie 3. The algorithm maintained target tracking despite many other targets entering the frame, including siphonophores and krill, which, in some cases, passed between the larvacean and the cameras. In summary, our attempts to minimize the vehicle's influence on the target were partially successful. The vehicle damaged the extremely fragile outer house, but the vehicle observed the animal for an extended period without disturbing the more robust inner house or the animal despite interference from other animals.

Another noteworthy aspect of the *Bathochordaeus* tracking can be seen in the second panel of Fig. 6, the depth plot. Although the animal appeared nearly motionless in the vehicle camera frame, the measured vehicle depth reveals that the animal and the vehicle moved vertically throughout the entire tracking exercise, following a wave with a 20-min period and 6-m amplitude. Depending on the species, zooplankton may either exhibit active depth keeping, or they may respond to the ocean's vertical dynamics much like a neutrally buoyant parcel of seawater (*61*, *62*). In this case, the animal appears to act as if it was neutrally buoyant. It was likely vertically displaced by an internal wave, which commonly occurs in Monterey Bay (*63*). This result is consistent with internal wave observations made using the M-AUE swarm off the coast of San Diego (*33*), although the M-AUE vehicles operated at constant depth and inferred the presence of an internal wave through temperature anomalies and changes in the spacing of the elements of the swarm.

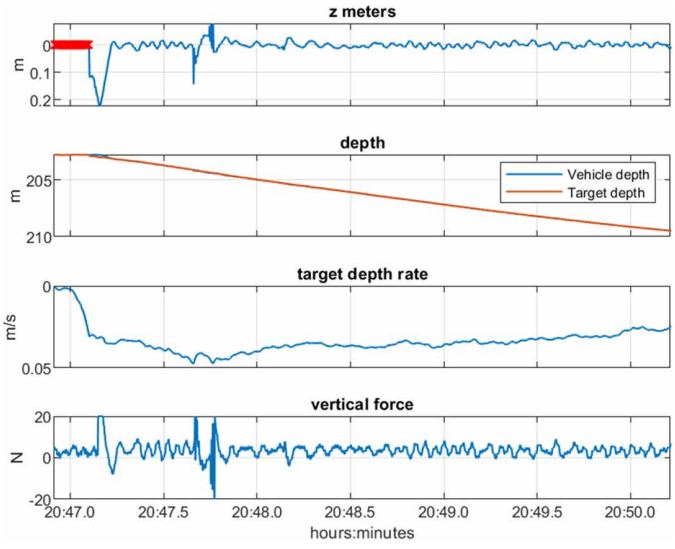

Fig. 5. At-sea *Solmissus* sp. tracking results. These plots document system performance while tracking a descending jellyfish *Solmissus* in the open ocean at a depth of about 200 m. Science camera and stereo tracking snapshots from this mission segment are shown at the top. The corresponding science video can be viewed in Movie 2. The *x* axes of the bottom panel show time in hours:minutes. The top time plot shows the target vertical position in the stereo frame. After acquiring the target, the vertical displacement in the stereo frame lagged slightly while maintaining an error of at most a few centimeters. Tracking was degraded at about 20:47.7 when the tracking algorithm briefly locked onto another target (a very bright, dynamic siphonophore), but the system was recovered. The middle panels show vehicle/target depth and depth rate, illustrating the near-steady motion of the target and vehicle. The bottom panel shows the vertical force, revealing a limit cycle that was low in magnitude (the full-scale thrust command is 60 N). During this tracking exercise, the vertical thrusters operated near the low end of their dynamic range.

Movie 3. *Bathochordaeus* tracking example. *Mesobot* actively tracked a larvacean *Bathochordaeus* (the tadpole-like animal) as it pumps water through its inner house while filter feeding. The total tracking period was more than 40 min, with 30 min of continuous tracking. While hydrodynamic disturbances from *Mesobot* destroyed the extremely fragile outer house shown in Fig. 4, we observed no disturbance of the more robust inner house or the animal. The tracking exercise was terminated because the vessel had to return to port.

While tracking, the thrust was typically very low despite the internal wave motion. Such low thruster activity results in minimal environmental disruption through either hydrodynamic or acoustic disturbance and results in low energy consumption. Review of the average power consumption during this tracking exercise (~70 W) and the overall vehicle battery pack capacity [~4 kilowatt-hour (kWh)] implies that the total mission time could have been more than 48 hours.

This result illustrates that we have achieved one of our major design goals: *Mesobot* can behave "almost Lagrangian." The vehicle tracked a seemingly motionless animal as it responded to dynamic oceanographic features. Although the observation was limited to 40 min due to operational constraints, the tracking was reliable and robust.

DISCUSSION

We designed *Mesobot* to enable observations of midwater organisms that are difficult or costly to observe using existing platforms. Such observations can improve our understanding of the behavior of midwater animals, which in turn improves our understanding of their role in the global carbon cycle and the potential impacts of increased exploitation. Our *Mesobot* design strives to make visual observations with minimal disruption, without evoking either attraction or avoidance of biological targets. The vehicle can track stationary and slow-moving animals using stereo cameras with either red or white lights and on-board algorithms. It can record high-quality HD and 4K video and 12 MP stills using low-light cameras. The vehicle has substantial auxiliary payload capacity to support additional sensors and samplers. More details about the vehicle and its sensors are presented later in Materials and Methods.

Our testing to date confirms many important design features of *Mesobot*. In tank tests, we showed that the system can lock onto, then track, moving organisms at speeds exceeding those of typical migrating zooplankton. In the open ocean at a depth of ~200 m, we demonstrated the vehicle's ability to track two species of zooplankton, the dinner plate jellyfish *Solmissus* sp. and the giant larvacean *B. stygius*. Power consumption during these tests projects an operational endurance exceeding 24 hours, which will enable the vehicle to study animals while they undergo diel migration and other daily movements.

The *Solmissus* sp. tracking experiment verified several key *Mesobot* attributes. The vehicle was able to track the animal while it moved vertically or horizontally. The thrust levels were modest, and we saw no indications that the animal was disturbed by the vehicle. The video showed several interesting aspects of the animal's behavior such as ramming, including a failed predation encounter with a siphonophore. Those observations also allowed the animal's motions to be precisely correlated to its swimming speed. Although our initial trials were relatively short, these results illustrate the potential insights we should gain from much longer surveys.

The tracking of the giant larvacean *B. stygius* confirmed other important *Mesobot* attributes. Although the vehicle's initial tracking disturbed the extremely fragile outer house, *Mesobot* was able to track the animal and its more resilient inner house without substantial disturbance for ~40 min as the animal engaged in filter feeding. Although the giant larvacean was not moving actively, the pressure readings show that the animal was following internal waves, rising and falling ±6 m over a ~20-min period. The animal appeared to be following the ocean dynamics much like a parcel of seawater. *Mesobot* matched those motions precisely using minimal thruster activity, illustrating the "near Lagrangian" behavior we hoped to create. JAMSTEC's *PICASSO* vehicle has achieved similar results, albeit for shorter periods (*64*).

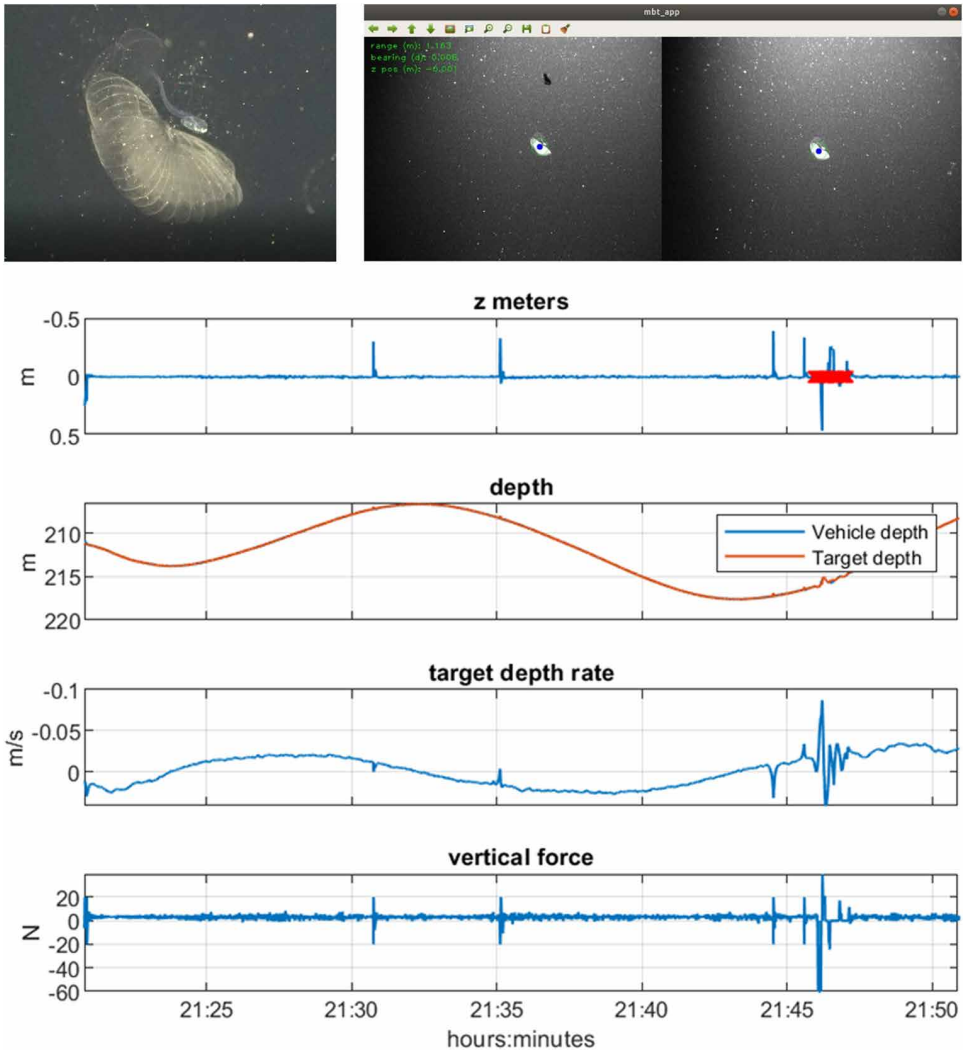

Fig. 6. At-sea larvacean tracking results. These plots show tracking results for a 30-min segment while tracking a larvacean (see Movie 3). Science camera and stereo tracking snapshots from this mission segment are shown at the top. As for the previous *Solmissus* example, the vertical displacement in the tracking frame converged quickly then remained at small values (on the order of 1 cm) with a few exceptions from which the system quickly recovered. The short segments of poor tracking were caused by new targets (siphonophores) entering the field of view; the longer segment about 21:46 was caused by our adjustments to the cameras and lights. In each case, the tracking was recovered. Adjustments to the tracking algorithm prevented interruption of tracking by the bright, fast-moving siphonophores as had occurred with the *Solmissus* example. The depth plot in the second panel shows that the target and vehicle moved vertically throughout the tracking exercise; most likely the animal was passively responding to an internal wave and acting like a parcel of ambient seawater. This result confirms that *Mesobot* can achieve near Lagrangian behavior when tracking a suitable target.

Our first in-water tracking experiences suggest a number of improvements. Although our tracking algorithm shows some robustness, tracking an animal over a full diel cycle will result in many challenges that we have not yet observed. We will use the datasets presented here as a training set for more modern object detection and tracking methods. Automatic recovery from a loss of tracking due to rapid target motion or overwhelming interference must also be improved.

We expect that *Mesobot* will emerge as a vital tool for observing midwater organisms. In addition to tracking animals for extended periods, we will be able to dispatch *Mesobot* to image and identify features observed from vessel biosonars. *Mesobot* is an ideal platform for implementing adaptive survey and sampling protocols, and we are learning much about how to minimize animal avoidance and attraction. *Mesobot* can survey and track midwater organisms while providing compelling imagery, which we hope will reveal previously unknown swimming behaviors, species interactions, morphological structures, and use of bioluminescence.

MATERIALS AND METHODS

Overall layout

The design of *Mesobot* prioritizes stable hovering and efficient vertical movement while enabling forward transit and accommodating a substantial auxiliary payload for other sensors and samplers. The vehicle is fully actuated; the thrusters can exert forces along and moments about all three body axes. The vehicle has high-static pitch and roll stability, with the buoyant elements placed high and the heavy, dense elements placed low. All thrusters, on adjustable mounts, were placed carefully so that they naturally create decoupled motions; accordingly, the forward and vertical thrusters induce minimal pitch moment. The control system does not actively change pitch or roll. The main thrusters for the forward/aft and vertical axes are low-powered (limited to under 60 W by the control electronics), slow-moving, and large-diameter thrusters to minimize hydrodynamic disturbances. The lateral thrusters that create heading moment and lateral (sway) force are small-diameter thrusters to fit into the limited available volume. Although the lateral thrusters create higher disturbance than the large thrusters, their thrust is directed sideways and not toward the volume imaged.

Thrusters and motor controllers

The thrusters for *Mesobot* must meet some unusual requirements compared with those used on conventional marine vehicles. For any battery-powered vehicle, efficiency will always be a concern. For *Mesobot*, additional constraints include creating minimal hydrodynamic disturbance, low-acoustic noise, and fine-scale thrust control to permit very stable hovering. Accordingly, we chose to use low-powered thrusters with large-diameter propellers to minimize hydrodynamic disturbance created by the vehicle (*65*, *66*). For an equivalent amount of input power, a larger-diameter propeller will be more efficient but will create a broader jet with lower translational and rotational velocity profiles

(*65*), which will in turn be less disruptive to the environment. Analogously, cargo vessels with larger, slower-turning propellers do less damage to harbor infrastructure when they accelerate compared with vessels with equivalent power applied to propellers with smaller diameters and higher shaft velocity (*66*).

Because no large-, low-powered thrusters were commercially available, *Mesobot's* thrusters and corresponding motor controllers are based on customized versions of commercially available products. They were specifically chosen and modified to support quiet, efficient operation and to enable thrust control over a wide dynamic range, which in turn supports smooth vehicle control with minimal limit cycling and reduced environmental disturbance compared with conventional thrusters. The core of the thrusters is motors from Blue Robotics T200 submersible thrusters that use pressure-tolerant brushless motors and normally drive a 79-mm-diameter propeller (*67*). Unlike most underwater vehicle thrusters that use oil-filled designs, these thrusters allow seawater to fill the gap between rotor and stator, relying on insulation to prevent electrical faults. In addition to simplicity, the lack of a shaft seal to separate the oil-filled volume from ambient seawater reduces friction and corresponding startup torque, thus improving the thruster dynamic range. The large-diameter *Mesobot* thrusters are Blue Robotics custom variants on the T200 thruster that include an 8:1 gear reduction and drive 46-cm propellers. The motor controllers are open-source VESC (Vedder Electronic Speed Controller) controllers (*68*) that feature sensorless commutation, which reduces the number of parts and minimizes the number of electrical connections (three wires versus six for typical motors with sensor-based commutation). In addition, VESC controllers support field-oriented control (*69*), which enables low acoustic noise and good torque control at very low shaft speeds. Because the VESC controllers are designed for larger motors (up to 240 A peak), the current sense resistors and corresponding firmware settings were adjusted to better measure current (maximum current, <6 A).

Cameras and lights

Mesobot (Fig. 7) carries a stereo pair of cameras used primarily for tracking and searching for targets, a color 4K video/still camera for scientific imagery, and a pair of commercially available light-emitting diode (LED) light arrays (*70*) that can emit either red (700 nm) or white light (~2500 K) at varying intensity under software control.

The stereo camera pair uses Allied Vision G-319B monochrome machine vision cameras with Gigabit Ethernet interfaces. These cameras have 1/1.8″ complementary metal-oxide semiconductor sensors with global shutters, which are critical to supporting synchronized operation in support of quantitative stereo imaging. The machine vision cameras have excellent sensitivity especially for red light and 2064 pixels (H) × 1544 pixels (V) resolution. They operate in commercial off-the-shelf (COTS) housings (Marine Imaging Technologies) with glass-domed optics, providing a 62° horizontal field of view and 47° vertical field of view. The cameras weigh 2.5 kg in air and 1.3 kg in water. They draw 2 W each at 12 V. These cameras were set up for a large depth of field, extending from just past the dome ports to infinity, thereby providing sharp focus without any real-time adjustment. The left camera faces directly forward, and the right camera is spaced at 0.28 m and rotated so that its field of view converges with the left camera's field of view 1.0 m ahead. The cameras were calibrated in water by acquiring image pairs of a calibration pattern. The MATLAB Stereo Calibrator App (*71*) was used to perform the final calibration.

Mesobot's science camera (Sony UMC-SC3A) provides high-quality color video (HD or 4K) and high-resolution stills (12 MP). The camera features a full-frame 35-mm sensor. The camera has outstanding low light capability (0.004 l× /ISO 409,600), compresses and records data to on-board memory, and is configured for remote control and limited viewing through a USB (universal serial port) port. Similar to the stereo cameras, this camera runs in a domed housing (Marine Imaging Technologies) weighing 11 kg in air and 10 kg in water and draws about 6 W at 12 VDC (volts direct current). A macro lens (Sony FE 90 mm F2.8 macro G OSS) supports operation through the dome without any additional corrective optics. The full-frame sensor not only provides high-resolution, sensitivity, and high-dynamic range but also creates a limited depth of field for reasonable f-stops. The field of view of the science camera is 27° wide and 17° high. The lights were pointed to converge at the focus point of the science camera (1 m forward), and baffles

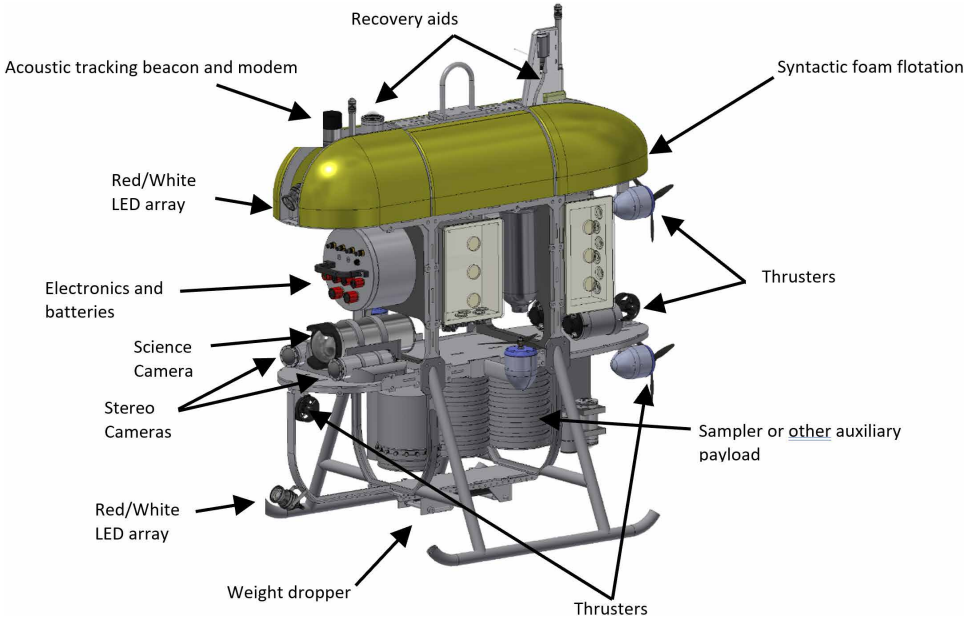

Fig. 7. *Mesobot* overview. This figure shows the vehicle with the protective side "skins" removed. For pitch and roll stability, the flotation material is at the top of the vehicle, and the heaviest components are low. The thrusters have adjustable mountings and have been positioned to minimize induced pitch and roll when forward and vertical thrust is applied. The large, slow-moving thrusters used for forward and vertical motion enable excellent servo control and result in little disturbance to the surrounding water. For recovery, the vehicle can drop up to 13 kg of steel weights. Those weights can also be released by a number of fail-safe mechanisms to ensure that the vehicle returns to the surface should unexpected failures occur. When the vehicle returns to the surface, its bright yellow upper section make it more visible, and it also carries three flashers, a VHF radio beacon, and a GPS/Iridium unit that transmits the vehicle's location via satellite.

were installed to prevent the out-of-focus near-field volume from being illuminated.

Tracking system

The tracking system provides real-time (10 Hz) updates of the target position (range, bearing, and vertical offset) using images from the stereo pair. The tracking results are passed to corresponding servo controllers, which close the appropriate loops to bring the target to the center of the tracking frame (zero bearing and vertical offset) while holding the range constant. The tracking methodologies used are based on the methodology presented in earlier jellyfish tracking work (*53*) but were updated to take advantage of advances in computing hardware and open-source software.

Although the on-board computing infrastructure has sufficient computational capability to support a variety of tracking algorithms, we chose to begin with a straightforward approach based on well-established methods and available software libraries that do not require training sets. Figure 8 illustrates results from the tracking algorithms, which can be summarized as follows:

1) A blob detector [OpenCV (*72*)] that isolates individual particulates and organisms from each camera view. The algorithm accepts a number of parameters for target size, threshold, and shape.

2) The suitability for tracking is then based on targets of sufficient size that have the smallest epipolar error (*53*). Constraints are also applied to disallow targets that move too quickly between frames. The epipolar calculations also provide the range, bearing, and vertical offset values, which are then transmitted to the servo system.

3) To deal with situations where the target moves out of the field of view, the algorithm maintains a "world frame" view of the target position based on the vehicle's heading. Should the target be lost, the control system attempts to reacquire the target based on the coordinates of that position.

From these initial field efforts, we now have data that we can use to develop training sets for object detection, classification, and tracking methods [e.g., YOLO (*73*, *74*) and SiamMask (*75*)]. These data sources can also be augmented by FathomNet, an open underwater image training set that leverages MBARI's 30-year expertly annotated Video Annotation and Reference System (*76*). Open-source implementations for these methods are well developed for *Mesobot*'s on-board computing environment (NVIDIA TX2). Although we anticipate many challenges due to specific aspects of *Mesobot's* imaging setup and the environment (e.g., uneven lighting and low-contrast targets that change shape markedly), the incorporation of machine learning into tracking algorithms should improve performance.

Control system

Mesobot's control system provides the necessary functions to monitor and control the sensors and actuators, to implement low-level servo control of heading and depth, to implement the automated processes such as programmed missions and automatic tracking, and to provide fail-safe responses should unexpected circumstances arise. The low-level functions (device interfaces and fail-safe responses) are implemented in a computing environment developed for MBARI's long-range AUVs (*31*). The LRAUV computing system provides an interface card (Load Controller Board) to each device, which implements the power and data communications interface (serial, analog, controller area network, etc.). The power control includes electronic switching, current monitoring, and ground fault detection.

The higher level control functions are implemented on an NVIDIA TX2 (*77*), a popular high-performance, low-powered graphic processing unit–based computer. The TX2 communicates with the

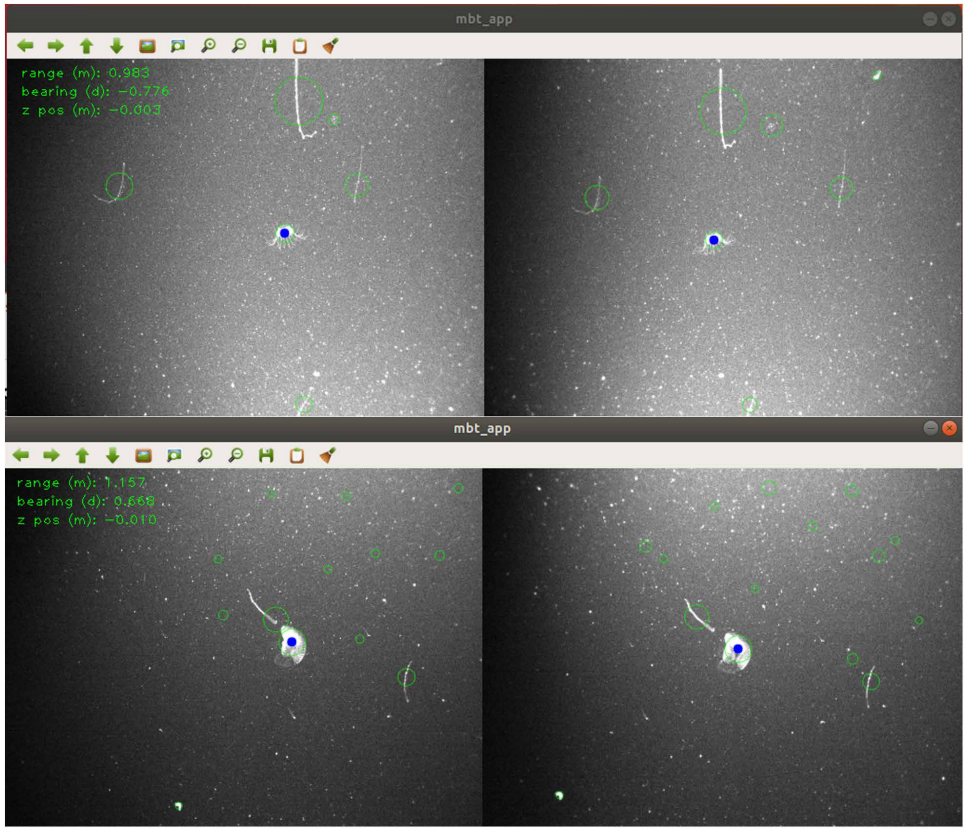

Fig. 8. Tracking algorithm overview. This figure illustrates the function of the tracking algorithms with snapshots from the jellyfish and larvacean tracking examples. These images are from the machine vision cameras that are used for stereo tracking. Blobs are independently identified in the left and right images, with blob size indicated by the green circles. Blobs are filtered by intensity, size, intensity, or inertia. Epipolar calculations are performed for all blob pairs in both images, and the pair with the lowest error is selected as the target. Those results are converted to range, bearing, and vertical offset and passed to the control system. The top panel shows an example while tracking *Solmissus*; the algorithm succeeds despite potential interference from marine snow and several siphonophores. The bottom panel shows an example from the larvacean tracking, where again the track remains on the desired animal despite the presence of several other prominent targets. The annotations in the top left-hand corner show the resolved tracking data, which were commanded for range 1.0 m, bearing 0°, and *z* position 0.0 m. This dataset will be used to train and test advanced object classifiers and tracking algorithms.

LRAUV computing system and the cameras through Ethernet connections, with data transfer implemented in Lightweight Communications and Marshalling (LCM) (*78*). Functions implemented on the TX2 and LRAUV computer include the following:

1) Thruster and sensor interfaces.

2) Background daemons for low-level monitoring of fault conditions and triggering appropriate responses (e.g., exceeding maximum mission depth, maximum mission time, seawater intrusion, etc.).

3) Thruster allocation: transformation from body forces/moments to individual thruster commands, including saturation logic.

4) Heading and depth servos: closed loop control of heading and depth when under joystick control, mission scripts, or tracking.

5) Mission scripting capability, enabling the vehicle to execute survey and sampling tasks.

Oceanographic sensors

Mesobot carries a suite of oceanographic sensors. These include a unit to measure conductivity, temperature, depth, and dissolved oxygen [Seabird GPCTD (*79*)] and an optical triplet [dual fluorometers and optical backscatter, Wet Labs ECO Puck (*80*)]. In addition to characterizing the environment in which *Mesobot* is operating, the sensor data are available to the control system in real time, enabling adaptive survey and sampling. *Mesobot* has a flexible payload bay, so it can carry a variety of sensors and samplers or be configured with only its core sensors.

Energy and power management

Mesobot carries a lithium-ion battery pack with a specified capacity of about 4.5 kWh driving a nominal 12-VDC power bus. The pack consists of 12 subpacks, which are each in turn composed of four commercial battery modules (Inspired Energy NH2034HD34). The decision to use a 12-VDC (4S) power bus allowed *Mesobot* to take advantage of existing LRAUV power control elements (*31*). A Woods Hole Oceanographic Institution–designed battery controller module on each subpack enables the 12 subpacks to be balanced internally and with each other when the batteries are charged. In real time, monitoring information can be used to automatically end a dive when the batteries reach a critical level. Eleven of the 12 subpacks are used in normal operation; the remaining pack is used as a reserve, which is used should the primary subpacks be depleted. The vehicle's power consumption during the active tracking phase of the dive averaged 93 W, so the battery pack provides enough energy for well more than 24 hours for a tracking mission with adequate reserves.

Lightweight fiber optic tether

Mesobot's tether uses 3-mm–outside diameter OFNR (Optical Fiber Nonconducting Riser) cable, which includes one buffered single-mode optical fiber, a Kevlar strength member, and a polyvinyl chloride jacket. Such cable is normally used to route fiber optic network connections in buildings when some strength and robustness are required, such as vertical runs between floors where the cable must support its own weight. Cables can be readily purchased from a number of vendors in any desired length complete with connectors. The tether is typically 50 m in length, and weights are attached midspan for predictable deployment.The tether is physically dropped from *Mesobot* at the end of each mission. The vehicle end has a modified ST (Straight Tip) termination (*81*), with the ST locking ring replaced by a magnet. A small motorized actuator on *Mesobot* extends nonmagnetic ejector pins, which push the tether cable out of the ST ferrule, allowing it to fall away from the vehicle. The tether is then recovered with the SmartClump for either reuse or disposal.

Recovery aids

Mesobot carries several features and devices to enable it to be located when it surfaces. First, the upper part of the vehicle is painted bright yellow, making it easier to see when on the surface. The vehicle carries three strobe lights to redundantly support night recoveries. A VHF radio beacon (*82*) can be detected when the vehicle surfaces and an approximate bearing determined with either a handheld or a ship-mounted radio direction finder. *Mesobot* also carries a Global Positioning System (GPS)/Iridium unit (*83*) that transmits the vehicle location over an Iridium satellite connection when the vehicle is on the surface. The resulting position fix can be read with a web browser provided the vessel has an internet connection. Should the vessel not have a working internet connection, the location can be received using a handheld Iridium terminal or ashore and the resulting fix communicated to the vessel by radio or satellite phone.

The vehicle is also equipped with a wireless network connection (Bullet M2HP). When the vehicle surfaces within ~1 km of the vessel, it automatically connects to the shipboard network, although at longer ranges the connection can often be lost depending on sea state. The wireless connection allows a human pilot to drive the vehicle toward the vessel and to make fine-scale maneuvers to help the deck crew attach a lift line onto the vehicle.

Last, the vehicle carries a set of drop weights, which can weigh up to ~13 kg in water. At the end of a dive, these are released using an electrically controlled "burn wire" backed up with a passive corrodible link. The release can be activated under program control or by a low-level self-powered deadman circuit that is engaged automatically should the primary computer system or main batteries fail.

Design summary

We have designed a marine robot to make observations of midwater targets unobtrusively, reducing effects that induce avoidance or attraction as much as possible. With endurance exceeding a full day, the vehicle can operate as a remotely operated or fully autonomous vehicle. Its automated tracking capabilities enable the vehicle to follow slow-moving targets, and we have demonstrated those capabilities on several species of zooplankton in the open ocean. Because these capabilities are not presently available, we anticipate that *Mesobot* will enable improved understanding of the complex daily lives of midwater animals. The vehicle carries a full suite of oceanographic sensors and has sufficient auxiliary payload capacity to carry other sensors and sampling devices. The vehicle also has a number of practical features for fail-safe return to the surface in response to faults and carries multiple radio and optical devices to aid in its recovery.

SUPPLEMENTARY MATERIALS

robotics.sciencemag.org/cgi/content/full/6/55/eabe1901/DC1
Fig. S1

REFERENCES AND NOTES

1. C. Robinson, D. K. Steinberg, T. R. Anderson, J. Arístegui, C. A. Carlson, J. R. Frost, J. F. Ghiglione, S. Hernández-León, G. A. Jackson, R. Koppelmann, B. Quéguiner, O. Ragueneau, F. Rassoulzadegan, B. H. Robison, C. Tamburini, T. Tanaka, K. F. Wishner,

J. Zhang, Mesopelagic zone ecology and biogeochemistry - A synthesis. *Deep Sea Res. II Top. Stud. Oceanogr.* **57**, 1504–1518 (2010).
2. X. Irigoien, T. A. Klevjer, A. Røstad, U. Martinez, G. Boyra, J. L. Acuña, A. Bode, F. Echevarria, J. I. Gonzalez-Gordillo, S. Hernandez-Leon, S. Agusti, D. L. Aksnes, C. M. Duarte, S. Kaartvedt, Large mesopelagic fishes biomass and trophic efficiency in the open ocean. *Nat. Commun.* **5**, 3271 (2014).
3. Porter Hoagland, D. Jin, M. Holland, K. Kostel, E. Taylor, N. Renier, M. Holmes, *Value Beyond View: Illuminating the Human Benefits of the Ocean Twilight Zone* (Woods Hole Oceanographic Institution, 2019); https://hdl.handle.net/1912/25013.
4. M. A. St. John, A. Borja, G. Chust, M. Heath, I. Grigorov, P. Mariani, A. P. Martin, R. S. Santos, A dark hole in our understanding of marine ecosystems and their services: Perspectives from the mesopelagic community. *Front. Mar. Sci.* **3**, 31 (2016).
5. P. Gaube, C. D. Braun, G. L. Lawson, D. J. McGillicuddy Jr., A. D. Penna, G. B. Skomal, C. Fischer, S. R. Thorrold, Mesoscale eddies influence the movements of mature female white sharks in the Gulf Stream and Sargasso Sea. *Sci. Rep.* **8**, 7363 (2018).
6. J. A. Goldbogen, D. E. Cade, D. M. Wisniewska, J. Potvin, P. S. Segre, M. S. Savoca, E. L. Hazen, M. F. Czapanskiy, S. R. Kahane-Rapport, S. L. DeRuiter, S. Gero, P. Tønnesen, W. T. Gough, M. B. Hanson, M. M. Holt, F. H. Jensen, M. Simon, A. K. Stimpert, P. Arranz, D. W. Johnston, D. P. Nowacek, S. E. Parks, F. Visser, A. S. Friedlaender, P. L. Tyack, P. T. Madsen, N. D. Pyenson, Why whales are big but not bigger: Physiological drivers and ecological limits in the age of ocean giants. *Science* **366**, 1367–1372 (2019).
7. P. Arranz, K. J. Benoit-Bird, A. S. Friedlaender, E. L. Hazen, J. A. Goldbogen, A. K. Stimpert, S. L. DeRuiter, J. Calambokidis, B. L. Southall, A. Fahlman, P. L. Tyack, Diving behavior and fine-scale kinematics of free-ranging Risso's dolphins foraging in shallow and deep-water habitats. *Front. Ecol. Evol.* **7**, 53 (2019).
8. K. O. Buesseler, C. H. Lamborg, P. W. Boyd, P. J. Lam, T. W. Trull, R. R. Bidigare, J. K. B. Bishop, K. L. Casciotti, F. Dehairs, M. Elskens, M. Honda, D. M. Karl, D. A. Siegel, M. W. Silver, D. K. Steinberg, J. Valdes, B. van Mooy, S. Wilson, Revisiting carbon flux through the ocean's twilight zone. *Science* **316**, 567–570 (2007).
9. K. Katija, R. E. Sherlock, A. D. Sherman, B. H. Robison, New technology reveals the role of giant larvaceans in oceanic carbon cycling. *Sci. Adv.* **3**, e1602374 (2017).
10. B. H. Robison, K. R. Reisenbichler, R. E. Sherlock, Giant larvacean houses: Rapid carbon transport to the deep sea floor. *Science* **308**, 1609–1611 (2005).
11. T. A. Klevjer, X. Irigoien, A. Røstad, E. Fraile-Nuez, V. M. Benítez-Barrios, S. Kaartvedt, Large scale patterns in vertical distribution and behaviour of mesopelagic scattering layers. *Sci. Rep.* **6**, 19873 (2016).
12. G. C. Hays, A review of the adaptive significance and ecosystem consequences of zooplankton diel vertical migrations. *Hydrobiologia* **503**, 163–170 (2003).
13. E. L. Cavan, E. C. Laurenceau-Cornec, M. Bressac, P. W. Boyd, Exploring the ecology of the mesopelagic biological pump. *Prog. Oceanogr.* **176**, 102125 (2019).
14. D. K. Steinberg, C. A. Carlson, N. R. Bates, S. A. Goldthwait, L. P. Madin, A. F. Michaels, Zooplankton vertical migration and the active transport of dissolved organic and inorganic carbon in the Sargasso Sea. *Deep Sea Res. Part I Oceanogr. Res. Pap.* **47**, 137–158 (2000).
15. B. H. Robison, K. R. Reisenbichler, R. E. Sherlock, The coevolution of midwater research and ROV Technology at MBARI. *Oceanography* **30**, 26–37 (2017).
16. H. Yoshida, D. J. Lindsay, H. Yamamoto, S. Tsukioka, T. Shimura, S. Ishibashi, Small hybrid vehicles for jellyfishes survey in midwater, in *ISOPE-I-07-292*, Lisbon, Portugal, January 2007, p. 5.
17. H. Yoshida, T. Aoki, H. Osawa, S. Tsukioka, S. Ishibashi, Y. Watanabe, J. Tahara, T. Miyazaki, T. Hyakudome, T. Sawa, K. Itoh, A. Ishikawa, D. Lindsay, Newly-developed devices for the two types of underwater vehicles, in *Proceedings of the OCEANS 2007 - Europe*, Aberdeen, UK, 18 to 21 June 2007, pp. 1–6.
18. Y. Zhang, J. P. Ryan, B. Kieft, B. W. Hobson, R. S. McEwen, M. A. Godin, J. B. Harvey, B. Barone, J. G. Bellingham, J. M. Birch, C. A. Scholin, F. P. Chavez, Targeted sampling by autonomous underwater vehicles. *Front. Mar. Sci.* **6**, 415 (2019).
19. P. H. Wiebe, M. C. Benfield, From the Hensen net toward four-dimensional biological oceanography. *Prog. Oceanogr.* **56**, 7–136 (2003).
20. P. H. Wiebe, G. L. Lawson, A. C. Lavery, N. J. Copley, E. Horgan, A. Bradley, Improved agreement of net and acoustical methods for surveying euphausiids by mitigating avoidance using a net-based LED strobe light system. *ICES J. Mar. Sci.* **70**, 650–664 (2013).
21. H. C. Rees, B. C. Maddison, D. J. Middleditch, J. R. M. Patmore, K. C. Gough, REVIEW: The detection of aquatic animal species using environmental DNA – A review of eDNA as a survey tool in ecology. *J. Appl. Ecol.* **51**, 1450–1459 (2014).
22. C. S. Davis, F. T. Thwaites, S. M. Gallager, Q. Hu, A three-axis fast-tow digital Video Plankton Recorder for rapid surveys of plankton taxa and hydrography. *Limnol. Oceanogr. Methods* **3**, 59–74 (2005).
23. L. Madin, E. Horgan, S. Gallager, J. Eaton, A. Girard, LAPIS: A new imaging tool for macro-zooplankton, in *Proceedings of the OCEANS 2006*, Boston, MA, 18 to 21 September 2006, pp. 1–5.
24. R. K. Cowen, C. M. Guigand, In situ ichthyoplankton imaging system (ISIIS): System design and preliminary results. *Limnol. Oceanogr. Methods* **6**, 126–132 (2008).
25. M. Picheral, L. Guidi, L. Stemmann, D. Karl, G. Id Daoud, G. Gorsky, The Underwater Vision Profiler 5: An advanced instrument for high spatial resolution studies of particle size spectra and zooplankton. *Limnol. Oceanogr. Methods* **8**, 462–473 (2010).
26. A. C. Lavery, P. H. Wiebe, T. K. Stanton, G. L. Lawson, M. C. Benfield, N. Copley, Determining dominant scatterers of sound in mixed zooplankton populations. *J. Acoust. Soc. Am.* **122**, 3304–3326 (2007).
27. A. C. Lavery, New platforms, technologies, and approaches for remote inference of physical and biological parameters using acoustic scattering techniques. *J. Acoust. Soc. Am.* **142**, 2598–2598 (2017).
28. R. Proud, N. O. Handegard, R. J. Kloser, M. J. Cox, A. S. Brierley, From siphonophores to deep scattering layers: Uncertainty ranges for the estimation of global mesopelagic fish biomass. *ICES J. Mar. Sci.* , 718–733 (2018).
29. D. Roemmich, G. Johnson, S. Riser, R. Davis, J. Gilson, W. B. Owens, S. Garzoli, C. Schmid, M. Ignaszewski, The argo program: Observing the global oceans with profiling floats. *Oceanography* **22**, 34–43 (2009).
30. R. E. Davis, C. E. Eriksen, C. P. Jones, Autonomous buoyancy-driven underwater vehicle gliders, in *Technology and Applications of Autonomous Underwater Vehicles*, G. Griffiths, Ed. (Taylor & Francis, London; New York, 2003), pp. 37–62.
31. B. W. Hobson, J. G. Bellingham, B. Kieft, R. McEwen, M. Godin, Y. Zhang, Tethys-class long range AUVs - Extending the endurance of propeller-driven cruising AUVs from days to weeks, in *Proceedings of the 2012 IEEE/OES Autonomous Underwater Vehicles (AUV)*, Southampton, UK, 24 to 27 September 2012, 24–2, pp. 1–8.
32. M. Furlong, D. Paxton, P. Stevenson, M. Pebody, S. D. Mcphail, J. Perrett, Autosub Long Range: A long range deep diving AUV for ocean monitoring, in *Proceedings of the 2012 IEEE/OES Autonomous Underwater Vehicles (AUV)*, Southampton, UK, 24 to 27 September 2012.
33. J. S. Jaffe, P. J. S. Franks, P. L. D. Roberts, D. Mirza, C. Schurgers, R. Kastner, A. Boch, A swarm of autonomous miniature underwater robot drifters for exploring submesoscale ocean dynamics. *Nat. Commun.* **8**, 14189–14189 (2017).
34. Franz Uiblein ED1 - Nuno A. Cruz, Deep-sea fish behavioral responses to underwater vehicles: Differences among vehicles, habitats and species, in *Autonomous Underwater Vehicles* (Rijeka: IntechOpen, 2011), p. Ch. 10.
35. L. Li, D. Stramski, R. A. Reynolds, Characterization of the solar light field within the ocean mesopelagic zone based on radiative transfer simulations. *Deep Sea Res. Part I Oceanogr. Res. Pap.* **87**, 53–69 (2014).
36. S. Kaartvedt, D. L. Aksnes, T. J. Langbehn, Enlightening the ocean's twilight zone. *ICES J. Mar. Sci.* **76**, 803–812 (2019).
37. R. B. Forward Jr., Diel vertical migration: Zooplankton photobiology and behaviour. *Oceanogr. Mar. Biol. Annu. Rev.* **26**, 361–393 (1988).
38. T. J. Langbehn, D. L. Aksnes, S. Kaartvedt, Ø. Fiksen, C. Jørgensen, Light comfort zone in a mesopelagic fish emerges from adaptive behaviour along a latitudinal gradient. *Mar. Ecol. Prog. Ser.* **623**, 161–174 (2019).
39. E. A. Widder, B. H. Robison, K. R. Reisenbichler, S. H. D. Haddock, Using red light for in situ observations of deep-sea fishes. *Deep Sea Res. Part Oceanogr. Res. Pap.* **52**, 2077–2085 (2005).
40. T. M. Frank, E. A. Widder, Comparative study of the spectral sensitivities of mesopelagic crustaceans. *J. Comp. Physiol. A.* **185**, 255–265 (1999).
41. F. de Busserolles, N. J. Marshall, Seeing in the deep-sea: Visual adaptations in lanternfishes. *Philos. Trans. R. Soc. Lond. Ser. B Biol. Sci.* **372**, 20160070 (2017).
42. E. A. Widder, M. I. Latz, P. J. Herring, J. F. Case, Far red bioluminescence from two deep-sea fishes. *Science* **225**, 512–514 (1984).
43. W. J. Stewart, A. Nair, H. Jiang, M. J. McHenry, Prey fish escape by sensing the bow wave of a predator. *J. Exp. Biol.* **217**, 4328–4336 (2014).
44. K. B. Catton, D. R. Webster, S. Kawaguchi, J. Yen, The hydrodynamic disturbances of two species of krill: Implications for aggregation structure. *J. Exp. Biol.* **214**, 1845–1856 (2011).
45. B. J. Gemmell, H. Jiang, J. R. Strickler, E. J. Buskey, Plankton reach new heights in effort to avoid predators. *Proc. Biol. Sci.* **279**, 2786–2792 (2012).
46. D. J. Lindsay, H. Yoshida, T. Uemura, H. Yamamoto, S. Ishibashi, J. Nishikawa, J. D. Reimer, R. J. Beaman, R. Fitzpatrick, K. Fujikura, T. Maruyama, The untethered remotely operated vehicle picasso-1 and its deployment from chartered dive vessels for deep sea surveys off okinawa, japan, and osprey reef, coral sea, Australia. *Mar. Technol. Soc. J.* **46**, 20–32 (2012).
47. R. K. Katzschmann, J. DelPreto, R. MacCurdy, D. Rus, Exploration of underwater life with an acoustically controlled soft robotic fish. *Sci. Robot.* **3**, eaar3449 (2018).
48. G. Polverino, M. Karakaya, C. Spinello, V. Soman, M. Porfiri, Behavioural and life-history responses of mosquitofish to biologically inspired and interactive robotic predators. *J. R. Soc. Interface* **16**, 20190359 (2019).

49. T. M. Grothues, A. E. Newhall, J. F. Lynch, K. S. Vogel, G. G. Gawarkiewicz, High-frequency side-scan sonar fish reconnaissance by autonomous underwater vehicles. *Can. J. Fish. Aquat. Sci.* **74**, 240–255 (2016).
50. G. B. Skomal, E. M. Hoyos-Padilla, A. Kukulya, R. Stokey, Subsurface observations of white shark *Carcharodon carcharias* predatory behaviour using an autonomous underwater vehicle. *J. Fish Biol.* **87**, 1293–1312 (2015).
51. A. L. Kukulya, R. Stokey, C. Fiester, E. M. H. Padilla, G. Skomal, Multi-vehicle autonomous tracking and filming of white sharks *Carcharodon carcharias*, in *Proceedings of th 2016 IEEE/OES Autonomous Underwater Vehicles (AUV)*, Tokyo, Japan, 6 to 9 November 2016, pp. 423–430.
52. H. Yoshida, D. J. Lindsay, H. Yamamoto, S. Ishibashi, T. Hyakudome, H. Okuno, T. Uemura, Development of the AUV/UROV 'PICASSO', in *ISOPE-I-08-367*, Vancouver, Canada, January 2008, p. 6.
53. J. H. Rife, S. M. Rock, Design and validation of a robotic control law for observation of deep-ocean jellyfish. *IEEE Trans. Robot.* **22**, 282–291 (2006).
54. S. Ishibashi, H. Yoshida, D. J. Lindsay, H. Yamamoto, T. Hyakudome, T. Sawa, H. Okuno, T. Uemura, An underwater vehicle for the tracking marine organism 'PICASSO', in *OMAE2009, Volume 4: Ocean Engineering; Ocean Renewable Energy; Ocean Space Utilization, Parts A and B*, May 2009, pp. 1495–1502.
55. P. H. Wiebe, N. J. Copley, S. H. Boyd, Coarse-scale horizontal patchiness and vertical migration of zooplankton in Gulf Stream warm-core ring 82-H. *Deep Sea Res. Part Oceanogr. Res. Pap.* **39**, S247–S278 (1992).
56. T. Cardoza, Research vessel *Rachel Carson*, in *MBARI*, 24 November 2015; www.mbari.org/at-sea/ships/rv-rachel-carson/ [accessed 13 January 2020].
57. H.-H. Chen, In-situ alignment calibration of attitude and ultra short baseline sensors for precision underwater positioning. *Ocean Eng.* **35**, 1448–1462 (2008).
58. K. Raskoff, Foraging, prey capture, and gut contents of the mesopelagic narcomedusa *Solmissus* spp. (Cnidaria: Hydrozoa). *Mar. Biol.* **141**, 1099–1107 (2002).
59. W. M. Hamner, B. H. Robison, In situ observations of giant appendicularians in Monterey Bay. *Deep Sea Res. Part Oceanogr. Res. Pap.* **39**, 1299–1313 (1992).
60. K. Katija, G. Troni, J. Daniels, K. Lance, R. E. Sherlock, A. D. Sherman, B. H. Robison, Revealing enigmatic mucus structures in the deep sea using DeepPIV. *Nature* **583**, 78–82 (2020).
61. A. Genin, J. S. Jaffe, R. Reef, C. Richter, P. J. S. Franks, Swimming against the flow: A mechanism of zooplankton aggregation. *Science* **308**, 860–862 (2005).
62. P. J. S. Franks, J. C. Garwood, M. Ouimet, J. Cortes, R. C. Musgrave, A. J. Lucas, Stokes drift of plankton in linear internal waves: Cross-shore transport of neutrally buoyant and depth-keeping organisms. *Limnol. Oceanogr.* **65**, 1286–1296 (2019).
63. F. Cazenave, Y. Zhang, E. McPhee-Shaw, J. Bellingham, T. Stanton, High-resolution surveys of internal tidal waves in Monterey Bay, California, using an autonomous underwater vehicle. *Limnol. Oceanogr. Methods* **9**, 571–581 (2011).
64. D. Lindsay, H. Yoshida, S. Ishibashi, M. Umetsu, A. Yamaguchi, H. Yamamoto, J. Nishikawa, J. D. Reimer, H. Watanabe, K. Fujikura, T. Maruyama, The uROV PICASSO, the Visual Plankton Recorder, and other attempts to image plankton, in *Proceedings if the 2013 IEEE International Underwater Technology Symposium (UT)*, Tokyo, Japan, 5 to 8 March 2013, pp. 1–3.
65. W. Lam, G. A. Hamil, Y. C. Song, D. J. Robinson, S. Raghunathan, A review of the equations used to predict the velocity distribution within a ship's propeller jet. *Ocean Eng.* **38**, 1–10 (2011).
66. B. Sumer, J. Fredsoe, The mechanics of scour in the marine environment. Advanced Series in Ocean Engineering. *World Sci.* **17**, 423–441 (2002).
67. R. F. Jehangir, J. A. Spadola, "Electric submersible thruster," US9963212B2 2018.
68. VESC Project; https://vesc-project.com/ [accessed 11 January 2020].
69. J. P. John, S. S. Kumar, B. Jaya, Space vector modulation based field oriented control scheme for brushless DC motors, in *Proceedings of the 2011 International Conference on Emerging Trends in Electrical and Computer Technology*, Nagercoil, India, 23 to 24 March 2011, pp. 346–351.
70. Multiray LED SeaLite (LSL-2025) - DeepSea Power & Light; www.deepsea.com/portfolio-items/multiray-led-sealite/ [accessed 11 January 2020].
71. Stereo Camera Calibrator App - MATLAB & Simulink; www.mathworks.com/help/vision/ug/stereo-camera-calibrator-app.html [accessed 23 January 2020].
72. OpenCV; https://opencv.org/ [accessed 13 January 2020].
73. J. Redmon, S. K. Divvala, R. B. Girshick, A. Farhadi, You only look once: Unified, real-time object detection. arXiv:1506.02640 (8 June 2015).
74. A. Bochkovskiy, C.-Y. Wang, H.-Y. M. Liao, YOLOv4: Optimal speed and accuracy of object detection. arXiv:2004.10934 (23 April 2020).
75. Q. Wang, L. Zhang, L. Bertinetto, W. Hu, P. H. S. Torr, Fast online object tracking and segmentation: A unifying approach. arXiv:1812.05050 (5 May 2019).
76. O. Boulais, B. Woodward, B. Schlining, L. Lundsten, K. Barnard, K. C. Bell, K. Katija, FathomNet: An underwater image training database for ocean exploration and discovery. arXiv:2007.00114 (10 July 2020).
77. Jetson TX2 Module, in *NVIDIA Developer*, 1 May 2017; https://developer.nvidia.com/embedded/jetson-tx2 [accessed 11 January 2020].
78. A. S. Huang, E. Olson, D. C. Moore, LCM: Lightweight Communications and Marshalling, in *2010 IEEE/RSJ International Conference on Intelligent Robots and Systems* (IEEE, 2010), pp. 4057–4062.
79. Glider Payload CTD (GPCTD) | Sea-Bird Scientific - Overview | Sea-Bird, 11 January 2020; www.seabird.com/moving-platform/glider-payload-ctd-gpctd/family?productCategoryId=54627473789 [accessed 11 January 2020].
80. ECO Triplet-w | Sea-Bird Scientific - Overview | Sea-Bird, 11 January 2020; www.seabird.com/combination-sensors/eco-triplet-w/family?productCategoryId=54627869918 [accessed 11 January 2020].
81. T. D. Mathis, C. M. Miller, "Optical fiber connector," US4934785A, 19 June 1990.
82. MetOcean NOVATECH Beacons and Flashers; www.metocean.com/product/mmb-7500/.
83. Apollo Beacon | Submersible Iridium GPS-LED Flasher Combo, 20 January 2020; https://xeostech.com/apollo [accessed 20 January 2020].

Acknowledgments: L. Madin (WHOI) played a fundamental role in the original *Mesobot* concept. M. J. Stanway (Otter Works LLC) contributed experience with the LRAUV computing infrastructure and developed much of the real-time software infrastructure including critical fail-safe processes and device interfaces. C. Machado (WHOI) contributed mechanical design details. We are indebted to the crew of RV *Rachel Carson* for excellent ship handling and seamanship. **Funding:** The design, construction, and initial testing for *Mesobot* was funded by the U.S. NSF program for Ocean Technology and Interdisciplinary Coordination (OTIC) award 1636575 and included developments supported by the David and Lucile Packard Foundation. Further development and testing were supported by the Woods Hole Oceanographic Institution's Ocean Twilight Zone (OTZ) Project, funded as part of The Audacious Project housed at TED. Development of the initial *Mesobot* concept was supported by the Walter A. and Hope Noyes Smith family. K.K. received funding from the Packard Foundation and NSF award 1636527. **Author contributions:** D.R.Y. was the lead principal investigator on the NSF and *Mesobot* component of OTZ, led the design and testing efforts, and composed low-level and mission control code. A.F.G., J.K.L., P.H.W., K.K., B.H.R., and S.M.R. were co-principal investigators on the NSF project. All coauthors actively participated in concept development, specifications of scientific requirements, resulting engineering design, and contributed to the analysis of field data and the writing of the manuscript. J.F. led the mechanical design effort including the detailed structural design and fabrication scheme, M.C. contributed to mechanical design, developed and tested thruster concept, and adapted open-source motor controllers. D.G.-I. developed the electronic design, wireless network, battery controllers, and fiber-optic tether concept. J.C.H. specified and implemented the camera systems, imaging and control software, network, and topside user interfaces. A.F.G., P.H.W., J.K.L., K.K., and B.H.R. contributed detailed scientific requirements for imaging, sensing, and sampling. K.K. and B.W.H. contributed to overall system engineering, computing systems, and operational methods. S.M.R. and M.R. developed and tested the tracking software. **Competing interests:** The authors declare that they have no competing interests. **Data and materials availability:** Video segments, dive metadata, data file descriptor, and vehicle sensor and state data files are available on the open-source repository: https://doi.org/10.6084/m9.figshare.12719837.

Submitted 5 August 2020
Accepted 24 May 2021
Published 16 June 2021
10.1126/scirobotics.abe1901

Citation: D. R. Yoerger, A. F. Govindarajan, J. C. Howland, J. K. Llopiz, P. H. Wiebe, M. Curran, J. Fujii, D. Gomez-Ibanez, K. Katija, B. H. Robison, B. W. Hobson, M. Risi, S. M. Rock, A hybrid underwater robot for multidisciplinary investigation of the ocean twilight zone. *Sci. Robot.* **6**, eabe1901 (2021).

Science Robotics

A hybrid underwater robot for multidisciplinary investigation of the ocean twilight zone

Dana R. Yoerger, Annette F. Govindarajan, Jonathan C. Howland, Joel K. Llopiz, Peter H. Wiebe, Molly Curran, Justin Fujii, Daniel Gomez-Ibanez, Kakani Katija, Bruce H. Robison, Brett W. Hobson, Michael Risi, and Stephen M. Rock

Sci. Robot. **6** (55), eabe1901. DOI: 10.1126/scirobotics.abe1901

Science Robotics (ISSN 2470-9476) is published by the American Association for the Advancement of Science. 1200 New York Avenue NW, Washington, DC 20005. The title *Science Robotics* is a registered trademark of AAAS.